

# Low-temperature vortex liquid in $\text{La}_{2-x}\text{Sr}_x\text{CuO}_4$

LU LI<sup>1\*</sup>, J. G. CHECKELSKY<sup>1</sup>, SEIKI KOMIYA<sup>2</sup>, YOICHI ANDO<sup>2</sup> AND N. P. ONG<sup>1\*</sup>

<sup>1</sup>Department of Physics, Princeton University, Princeton, New Jersey 08544, USA

<sup>2</sup>Central Research Institute of Electric Power Industry, Komae, Tokyo 201-8511, Japan

\*e-mail: luli@princeton.edu; npo@princeton.edu

Published online: 18 March 2007; doi:10.1038/nphys563

**In copper oxide superconductors, the lightly doped (small dopant concentration,  $x$ ) region is of major interest<sup>1,2</sup> because superconductivity, antiferromagnetism and the pseudogap state come together near a critical doping value,  $x_c$ . But the way in which superconductivity is destroyed as  $x$  is decreased at very low temperatures,  $T$ , is not clear<sup>3–7</sup>. Does the pair condensate vanish abruptly at a critical value,  $x_c$ ? Or is phase coherence of the condensate destroyed by spontaneous vortices—as is the case at elevated  $T$  (refs 8–10)? So far, magnetization data at low  $T$  are very sparse in this region of the phase diagram. Here, we report torque magnetometry measurements on  $\text{La}_{2-x}\text{Sr}_x\text{CuO}_4$ , which show that, in zero magnetic field, quantum phase fluctuations destroy superconductivity at  $x_c \approx 0.055$ . The phase-disordered condensate survives to  $x = 0.03$ . In finite field  $H$ , the vortex solid-to-liquid transition occurs at  $H$  lower than the depairing field,  $H_{c2}$ . The resulting phase diagram reveals the large fraction of the  $x$ – $H$  plane occupied by the quantum vortex liquid.**

In underdoped  $\text{La}_{2-x}\text{Sr}_x\text{CuO}_4$  (LSCO), the magnetic susceptibility is dominated by the Curie-like spin susceptibility and the van Vleck orbital susceptibility<sup>11–13</sup>. These strongly  $T$ -dependent terms render weak diamagnetic signals difficult to detect using standard magnetometry. However, because the spin susceptibility is nearly isotropic<sup>13</sup> whereas the incipient diamagnetism is anisotropic, torque magnetometry has proved to be effective in resolving the diamagnetic signal<sup>14–17</sup> (the resistivity anisotropy is 6,000–8,000 below 40 K, so the supercurrent is predominantly in-plane; see Supplementary Information). With  $\mathbf{H}$  tilted at a slight angle,  $\phi$ , to the crystal  $c$  axis, the torque,  $\tau$ , may be expressed as an effective magnetization,  $M_{\text{obs}} \equiv \tau/\mu_0 H_x V$ , where  $V$  is the sample volume,  $\mu_0$  is the permeability and  $H_x = H \sin \phi$  (we take  $\mathbf{z} \parallel \mathbf{c}$ ). In cuprates,  $M_{\text{obs}}$  comprises three terms<sup>14,15</sup>

$$M_{\text{obs}}(T, H_x) = M_d(T, H_x) + \Delta M_s(T, H_x) + \Delta \chi^{\text{orb}}(T)H_x \quad (1)$$

where  $M_d(T, H_x)$  is the diamagnetic magnetization of interest,  $\Delta M_s$  is the anisotropy of the spin local moments and  $\Delta \chi^{\text{orb}}$  is the anisotropy of the van Vleck orbital susceptibility (see the Supplementary Information).

We label the seven samples studied as 03 (with  $x = 0.030$ ), 04 (0.040), 05 (0.050), 055 (0.055), 06 (0.060), 07 (0.070) and 09 (0.090). To start, we confirmed that, above  $\sim 25$  K,  $M_{\text{obs}}$  derived from the torque experiment in sample 03 is in good, quantitative agreement with the anisotropy inferred from previous

bulk susceptibility measurements<sup>13</sup> on a large crystal of LSCO ( $x = 0.03$ ) (see the Supplementary Information).

Figure 1 shows the magnetization,  $M_{\text{obs}}$ , in samples 055 and 06. The pattern of  $M_{\text{obs}}$  results from the sum of the three terms in equation (1). Figure 1a shows how it evolves in sample 055. At high  $T$  (60–200 K), the curves of  $M_{\text{obs}}$  versus  $H$  are fan-like, reflecting the weak  $T$  dependence<sup>14</sup> of the orbital term  $\Delta \chi^{\text{orb}}(T)H$ . At the onset temperature for diamagnetism,  $T_{\text{onset}}$  (55 K, bold curve), the diamagnetic term,  $M_d$ , appears as a new contribution. The strong  $H$  dependence of  $M_d$  causes  $M_{\text{obs}}$  to deviate from the  $H$ -linear behaviour. In Fig. 1b, the evolution is similar, except that the larger diamagnetism forces  $M_{\text{obs}}$  to negative values at low  $H$ . As mentioned, the spin contribution,  $\Delta M_s$ , is unresolved above  $\sim 40$  K in both panels. To magnify the diamagnetic signal, we subtract the orbital term,  $\Delta \chi^{\text{orb}}H$  (the three terms are also apparent in the total observed susceptibility  $\chi_{\text{obs}} = M_{\text{obs}}/H$ ; see the Supplementary Information).

The resulting curves,  $M'_{\text{obs}}(T, H) \equiv M_{\text{obs}} - \Delta \chi^{\text{orb}}H$ , are shown for sample 05 in Fig. 1c. At low fields,  $M'_{\text{obs}}$  shows an interesting oscillatory behaviour (curves at 0.5 and 0.75 K), but at high fields it tends towards saturation. By examining how  $M'_{\text{obs}}$  behaves in the two limits of weak and intense fields (see the Supplementary Information), we have found that  $M'_{\text{obs}}$  comprises a diamagnetic term,  $M_d(T, H)$ , that resembles the ‘tilted hill’ profile of diamagnetism in the vortex-liquid state above the critical temperature,  $T_c$ , reported previously<sup>10,14</sup>, and a spin-anisotropy term,  $\Delta M_s$ .

Modelling the latter as free spin-1/2 local moments with anisotropic  $g$  factors measured with  $\mathbf{H} \parallel \mathbf{c}$  ( $g_c$ ) and  $\mathbf{H} \perp \mathbf{c}$  ( $g_{ab}$ ), we have (see the Supplementary Information)

$$\Delta M_s(T, H) = P(T) \tanh(\beta g_{\phi} \mu_B B/2) \quad (2)$$

where  $\mu_B$  is the Bohr magneton,  $\beta = 1/k_B T$  and  $g_{\phi} = \sqrt{(g_c \cos \phi)^2 + (g_{ab} \sin \phi)^2}$  ( $k_B$  is Boltzmann’s constant). With  $g_{\phi} \sim g_c$  fixed at 2.1, the sole adjustable parameter at each  $T$  is the prefactor  $P(T)$ . Equation (2) accounts very well for the curves in Fig. 1c, especially the oscillatory behaviour; at  $T = 0.5$  and 0.75 K,  $\Delta M_s \sim 1/k_B T$  dominates  $M_d$  in weak  $H$ , but for  $H > k_B T/g_c \mu_B$ , the saturation of  $\Delta M_s$  implies that  $M'_{\text{obs}}(H)$  adopts the profile of  $M_d(H)$  apart from a vertical shift. Lightly doped LSCO enters a spin- or cluster-glass state<sup>11,12</sup> below the spin-glass temperature,  $T_{\text{sg}}$ , which is sensitive to sample purity (in 03 and 04,  $T_{\text{sg}} \sim 2.5$  and 1 K, respectively).

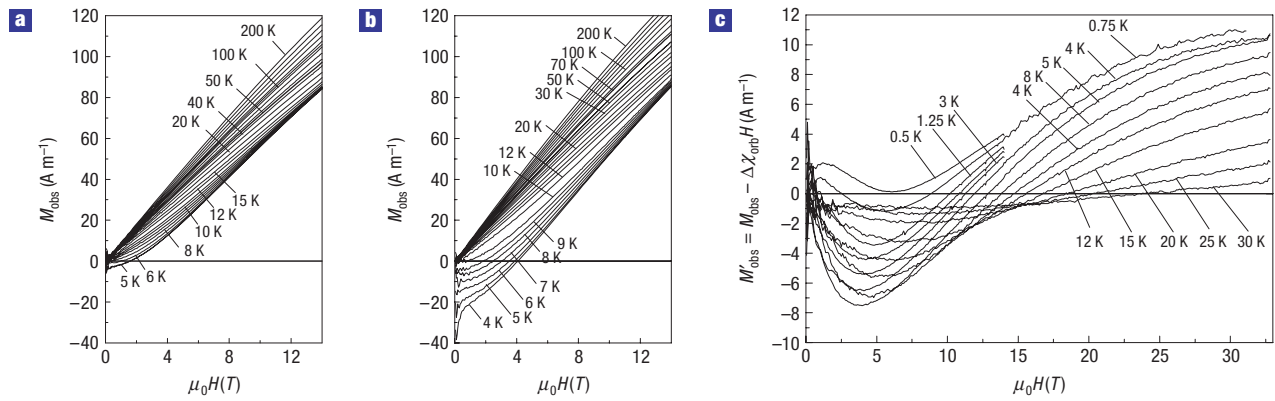


**Figure 1** Magnetization curves in lightly doped LSCO. **a**, Curves in sample 055 ( $T_c \sim 0.5$  K) at  $T = 4\text{--}200$  K. **b**, Curves in 06 ( $T_c \sim 5$  K). The crystal is glued to the tip of the cantilever with its  $c$  axis at a small angle,  $\phi \sim 15^\circ$ , to the field  $H$  (we write  $H_z$  as  $H$ ). Above  $T_{\text{onset}}$  (bold curves at 55 and 70 K in **a** and **b**, respectively), the fan-like pattern is due entirely to the paramagnetic term,  $\Delta\chi^{\text{orb}}(T)H$  (see the Supplementary Information for a plot of  $\Delta\chi^{\text{orb}}(T)$ ). Below  $T_{\text{onset}}$ , the diamagnetic term,  $M_d$ , becomes evident. **c**, The profiles of  $M'_{\text{obs}} = M_{\text{obs}} - \Delta\chi^{\text{orb}}H$  in sample 05. Note the oscillation in weak  $H$  at  $T = 0.5$  and 0.75 K and the approach towards saturation in high fields. These curves are separated into  $\Delta M_s$  and  $M_d$  in Fig. 2b.

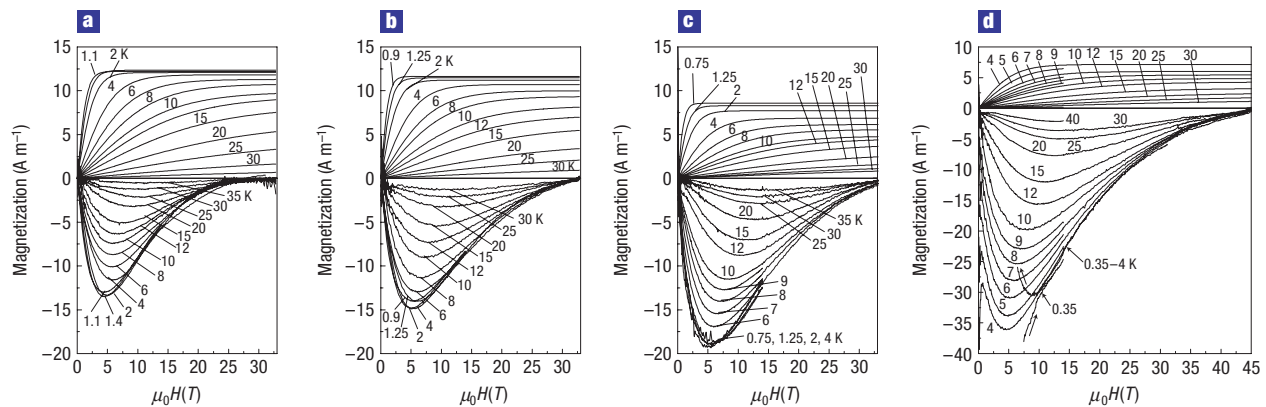


**Figure 2** Separation of magnetization into the spin term,  $\Delta M_s(T, H)$ , and the diamagnetic term,  $M_d(T, H)$ . **a–d**, Curves of  $\Delta M_s$  (positive) and  $M_d$  (negative) versus  $H$  in samples 04 (**a**), 05 (**b**), 055 (**c**) and 06 (**d**). In each sample, the diamagnetic minimum (at 5 T) deepens rapidly between 30 and 5 K, but does not change below  $T_0$ . The depairing field,  $H_{c2}$ , is estimated to be 25, 35, 43 and 48 T in **a–d**, respectively. In **d**, the branching curves (with arrows) indicate the high-field limit of the vortex solid at 0.35 K. Above  $H_{\text{irr}}(T)$ , the low- $T$  curves merge with the vortex-liquid curve at 4 K.

Subtracting  $\Delta M_s$  from  $M'_{\text{obs}}$ , we isolate the purely diamagnetic term,  $M_d(T, H)$ . Figure 2 shows the curves of  $M_d$  and  $\Delta M_s$  at selected  $T$  in samples 04, 05, 055 and 06. Samples 03, 04 and 05 do not show any Meissner effect. The strict reversibility of the  $M_d$ – $H$  curves confirms that we are in the vortex-liquid state in 03, 04 and 05. When  $x$  exceeds  $x_c$ , the samples exhibit broad Meissner transitions ( $T_c \sim 0.5$  and 5 K in 055 and 06, respectively). Hysteretic behaviour appears below a strongly  $T$ -dependent irreversibility field,  $H_{\text{irr}}(T)$ , discussed below. The  $T$  dependences in the four panels reveal an important pattern. In the vortex liquid, the overall magnitude of  $M_d$  grows rapidly as we cool from 35 to 5 K, but it stops changing below a crossover temperature,  $T_Q$  ( $\sim 4$  K in samples 05, 055 and 06, and  $\sim 2$  K in 04). Even in sample 06, where  $H_{\text{irr}} \sim 9$  T at 0.35 K,  $M_d$  recovers the  $T$ -independent profile when  $H > H_{\text{irr}}$  (diverging branches at 9 T in Fig. 2d). The insensitivity to  $T$  suggests that the excitations, which degrade the diamagnetic response in the liquid state, are governed by quantum statistics below  $T_Q$ .

In intense fields, the field suppression of  $M_d$  provides an estimate of the depairing field,  $H_{c2}$  ( $\sim 20, 25, 35, 43$  and 48 T in samples 03, 04, 05, 055 and 06, respectively). We find that  $H_{c2}$  is nominally  $T$  independent<sup>14</sup>. The remarkably large values of  $H_{c2}$  at such low hole densities imply that the pair-binding energy is anomalously large down to  $x = 0.03$ . In high fields, a sizeable diamagnetic signal is seen, but long-range phase rigidity (in zero  $H$ ) is absent down to  $T = 0.35$  K unless  $x$  exceeds  $x_c$ . At low  $T$ , this transition is quite abrupt. Next, we discuss the vortex solid and the phase diagram.

Hysteresis in  $M_d$  versus  $H$  below  $H_{\text{irr}}(T)$  provides a sensitive indication of the presence of the vortex solid. The strong vortex pinning in LSCO leads to large hystereses as soon as the vortex system exhibits shear rigidity. The hysteretic loops, which appear in sample 055, expand very rapidly as  $x$  exceeds 0.055. By examining the hysteretic loops (Fig. 3a shows curves for 06), we can determine  $H_{\text{irr}}(T)$  quite accurately. Vortex avalanches—signatures of the vortex solid—are observed (for

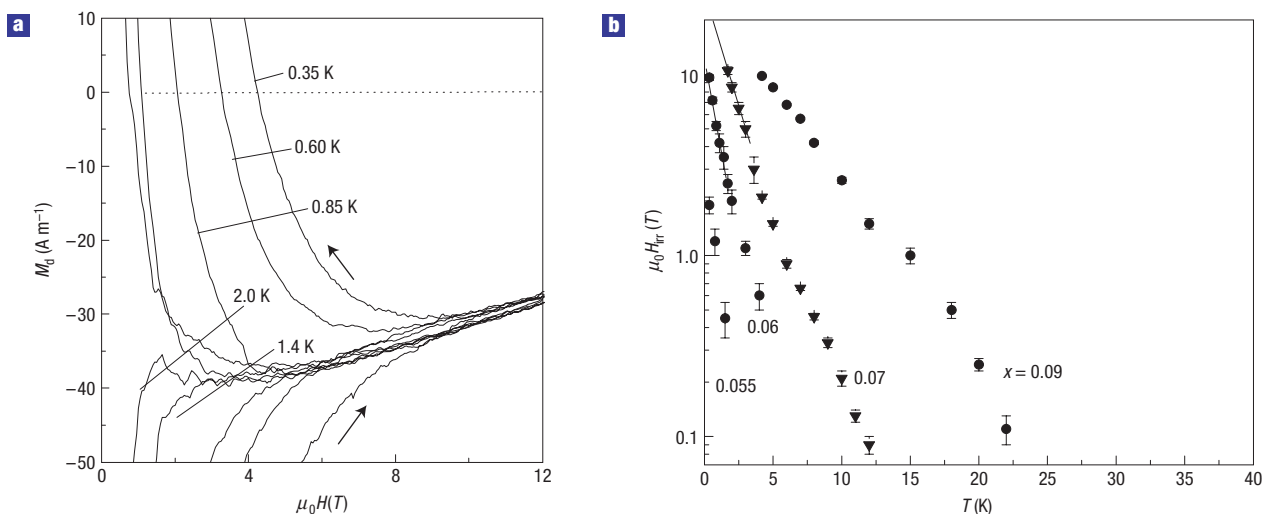


**Figure 3** The hysteresis curves and irreversibility field  $H_{\text{irr}}(T)$  in the vortex-solid phase. **a**, The hysteretic curves of  $M_d$  versus  $H$  in sample 06 at  $T$  from 0.35 to 2 K. Although the hysteretic segments for  $H < H_{\text{irr}}(T)$  are very strongly  $T$  dependent, the reversible segments above  $H_{\text{irr}}(T)$  are not. The latter match the  $T$ -constant profile shown in Fig. 2d. **b**, The  $T$  dependences of  $H_{\text{irr}}(T)$  in samples 055, 06, 07 and 09 in semilog scale. At low  $T$ , the data approach equation (3). The steep decrease of the characteristic temperature  $T_0$  as  $x \rightarrow x_c$  implies a softening of the vortex solid ( $T_0 \sim 1$  K in sample 06). The gradual convergence of the two branches of the irreversibility curves (see curves in **a**) leads to uncertainties in fixing  $H_{\text{irr}}(T)$  (shown as the error bars in **b**).

$H < H_{\text{irr}}$ ) unless the field-sweep rate is very slow (see the Supplementary Information).

The temperature dependence of  $H_{\text{irr}}(T)$  is plotted in Fig. 3b for samples  $x > x_c$ . At low  $T$ , the dependence approaches the exponential form

$$H_{\text{irr}}(T) = H_0 \exp(-T/T_0). \quad (3)$$

The parameters  $H_0$  and  $T_0$  decrease steeply as  $x \rightarrow x_c$ . The field parameter,  $H_0$ , provides an upper bound for the zero-Kelvin melting field,  $H_m(0)$ . Equation (3), reminiscent of the Debye–Waller factor, strongly suggests that the excitations responsible for the melting transition follow classical statistics at temperatures down to 0.35 K. The classical nature of these excitations contrasts with the quantum nature of the excitations in the vortex liquid below  $T_Q$  described above.

The inferred values of  $H_0$  (2, 13, 25 and 40 T in 055, 06, 07 and 09, respectively) are much smaller than  $H_{c2}(0)$ . Hence, after the vortex solid melts, there exists a broad field range in which the vortices remain in the liquid state at low  $T$ . The existence of the liquid at  $T < T_Q$  implies very large zero-point motion associated with a small vortex mass,  $m_v$ , which favours a quantum-mechanical description.

Finally, we construct the low- $T$  phase diagram in the  $x$ – $H$  plane. Figure 4 shows that the  $x$  dependence of  $H_{c2}(0)$ , the depairing field scale, is qualitatively distinct from that of  $H_0$ , the boundary of the vortex solid. The former varies roughly linearly with  $x$  between 0.03 and 0.07 with no discernible break-in-slope at  $x_c$ , whereas  $H_0$  falls steeply towards zero at  $x_c$  with large negative curvature. This sharp decrease—also reflected in the 1,000-fold shrinkage of the hysteresis amplitude between  $x = 0.07$  and 0.055 (see the Supplementary Information)—is strong evidence that the collapse of the vortex solid is a quantum critical transition. This is shown by examining the variation of  $H_{\text{irr}}$  versus  $x$  at several fixed  $T$  (dashed lines). At 4 K,  $H_{\text{irr}}$  approaches zero gently with positive curvature, but at lower  $T$ , the trajectories tend towards negative curvature. In the limit  $T = 0$ ,  $H_0$  approaches zero at  $x_c$  with a nearly

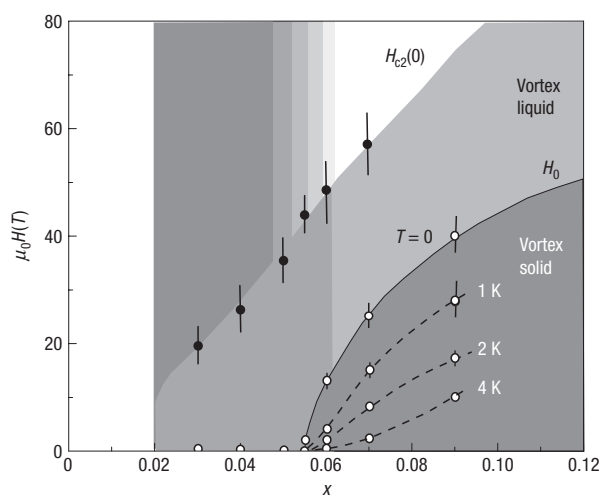


**Figure 4** The phase diagram of LSCO in the  $x$ – $H$  plane at low temperatures. The field  $H_0 = \lim_{T \rightarrow 0} H_{\text{irr}}$  (the boundary between vortex-solid and vortex-liquid states) falls steeply to zero as  $x \rightarrow x_c$  (solid curve). The dashed lines indicate the variation of  $H_{\text{irr}}(T)$  versus  $x$  at fixed  $T$ , as indicated. In contrast, the depairing field,  $H_{c2}(0)$  (closed circles), is nominally linear in  $x$ . Below  $x_c$ , the vortex liquid is stable and coexists with a growing magnetic background (graded shading). The error bars on  $H_{c2}(0)$  and  $H_0$  (vertical lines) are estimated uncertainties in field values. When the uncertainty in  $H_0$  is smaller than  $\pm 1$  T (nominal size of the open circles), the error bars are not shown.

vertical slope. The focusing of the trajectories to the point  $(x_c, 0)$  is characteristic of a sharp transition at  $x_c$ , and is strikingly different from the smooth decay suggested by viewing lightly doped LSCO as a system of superconducting islands with a broad distribution of  $T_c$  values.

In Fig. 4, the high-field vortex liquid is seen to extend continuously to  $x < x_c$  where it coexists with the cluster/spin-glass

state<sup>11,12</sup> (samples 03, 04 and 05). As shown in Fig. 2 (see the Supplementary Information), the robustness of  $M_d$  to intense fields attests to unusually large pairing energy even at  $x = 0.03$ , but the system stays as a vortex liquid down to 0.35 K.

In the limit  $H \rightarrow 0$ , the vortex liquid ( $x < x_c$ ) has equal populations of vortices and antivortices. This implies that, as  $x$  falls below  $x_c$  at low  $T$  and in zero field, superconductivity is destroyed by the spontaneous appearance of free (anti) vortices engendered by increased charge localization and strong phase fluctuation<sup>3,4,6</sup>. In zero field, superconductivity first transforms to a vortex-liquid state with strong phase disordering. The rapid growth of the spin-/cluster-glass state in LSCO suggests that incipient magnetism also plays a role in destroying superconductivity.

Received 14 November 2006; accepted 29 January 2007; published 18 March 2007.

## References

- Lee, P. A., Nagaosa, N. & Wen, X. G. Doping a Mott insulator: Physics of high-temperature superconductivity. *Rev. Mod. Phys.* **78**, 17–85 (2006).
- Anderson, P. W. Present status of the theory of the high- $T_c$  cuprates. *Low Temp. Phys.* **32**, 282–289 (2006).
- Doniach, S. Quantum fluctuations in two-dimensional superconductors. *Phys. Rev. B* **24**, 5063–5070 (1981).
- Fisher, M. P. A., Weichman, P. B., Grinstein, G. & Fisher, D. S. Boson localization and the superfluid-insulator transition. *Phys. Rev. B* **40**, 546–570 (1989).
- Fisher, M. P. A. & Lee, D. H. Correspondence between two-dimensional bosons and a bulk superconductor in a magnetic field. *Phys. Rev. B* **39**, 2756–2759 (1989).
- Melikyan, A. & Tešanović, Z. A model of phase fluctuations in a lattice  $d$ -wave superconductor: application to the Cooper pair charge-density-wave in underdoped cuprates. *Phys. Rev. B* **71**, 214511 (2005).
- Nikolic, P. & Sachdev, S. Effective action for vortex dynamics in clean  $d$ -wave superconductors. *Phys. Rev. B* **73**, 134511 (2006).
- Emery, V. J. & Kivelson, S. A. Importance of phase fluctuations in superconductors with small superfluid density. *Nature* **374**, 434–437 (1995).
- Wang, Y. *et al.* The onset of the vortex-like Nernst signal above  $T_c$  in  $\text{La}_{2-x}\text{Sr}_x\text{CuO}_4$  and  $\text{Bi}_2\text{Sr}_{2-x}\text{La}_x\text{CuO}_6$ . *Phys. Rev. B* **64**, 224519 (2001).
- Wang, Y., Li, L. & Ong, N. P. Nernst effect in high- $T_c$  superconductors. *Phys. Rev. B* **73**, 024510 (2006).
- Keimer, B. *et al.* Magnetic excitations in pure, lightly doped, and weakly metallic  $\text{La}_2\text{CuO}_4$ . *Phys. Rev. B* **46**, 14034–14053 (1992).
- Niedermayer, Ch. *et al.* Common phase diagram for antiferromagnetism in  $\text{La}_{2-x}\text{Sr}_x\text{CuO}_4$  and  $\text{Y}_{1-x}\text{Ca}_x\text{Ba}_2\text{CuO}_6$  as seen by muon spin rotation. *Phys. Rev. Lett.* **80**, 3843–3846 (1998).
- Lavrov, A. N., Ando, Y., Komiya, S. & Tsukada, I. Unusual magnetic susceptibility anisotropy in untwinned  $\text{La}_{2-x}\text{Sr}_x\text{CuO}_4$  single crystals in the lightly doped region. *Phys. Rev. Lett.* **87**, 017007 (2001).
- Wang, Y. *et al.* Field-enhanced diamagnetism in the pseudogap state of the cuprate  $\text{Bi}_2\text{Sr}_2\text{CaCu}_2\text{O}_{8+\delta}$  superconductor in an intense magnetic field. *Phys. Rev. Lett.* **95**, 247002 (2005).
- Li, L. *et al.* Strongly nonlinear magnetization above  $T_c$  in  $\text{Bi}_2\text{Sr}_2\text{CaCu}_2\text{O}_{8+\delta}$ . *Europhys. Lett.* **72**, 451–457 (2005).
- Farrell, D. E. *et al.* Experimental evidence for a transverse magnetization of the Abrikosov lattice in anisotropic superconductors. *Phys. Rev. Lett.* **61**, 2805–2808 (1988).
- Bergemann, C. *et al.* Superconducting magnetization above the irreversibility line in  $\text{Tl}_2\text{Ba}_2\text{CuO}_{6+\delta}$ . *Phys. Rev. B* **57**, 14387–14396 (1998).

## Acknowledgements

Valuable discussions with Y. Wang, Z. Tešanović, S. Sachdev, S. A. Kivelson, P. W. Anderson and J. C. Davis are acknowledged. The research at Princeton was supported by the National Science Foundation (NSF) through an MRSEC grant DMR 0213706. Research at CRIEPI was supported by a Grant-in-Aid for Science from the Japan Society for the Promotion of Science. The high-field measurements were carried out in the National High Magnetic Field Laboratory, Tallahassee, which is supported by NSF, the Department of Energy and the State of Florida. Correspondence and requests for materials should be addressed to L.L. or N.P.O. Supplementary Information accompanies this paper on [www.nature.com/naturephysics](http://www.nature.com/naturephysics).

## Competing financial interests

The authors declare no competing financial interests.

Reprints and permission information is available online at <http://npg.nature.com/reprintsandpermissions/>